Theor Chem Acc (2016) 135:63
DOI 10.1007/s00214-015-1803-7

REGULAR ARTICLE

Difluorodiazirine (CF_2N_2): a quantum mechanical study of the electron density and of the electrostatic potential in the ground and excited electronic states

Luiz Alberto Terrabuio[1,2] · Roberto Luiz Andrade Haiduke[1] · Chérif F. Matta[2,3,4]

Received: 24 November 2015 / Accepted: 29 December 2015 / Published online: 24 February 2016

Abstract The difluorocarbene radical (:CF_2), used in organic synthesis and in photoaffinity labeling, can be generated by the pyrolytic or photolytic decomposition of 3,3-difluorodiazirine (CF_2N_2, DFD). DFD possesses no dipole moment in the ground electronic state S_0 but has an experimental dipole of 1.5 ± 0.2 debye (D) in its first singlet excited state S_1. These observations have been ascribed to the shift in electron population between orbitals (Frenking et al. in J Comp Chem 28:117–126, 2007). An alternative real-space explanation is presented, which shows that the vanishing dipole moment in S_0 results from a balance between a charge transfer contribution due to the flow of charge between atoms and an atomic polarization term due to the non-sphericity of atoms in molecules. This balance is altered in S_1. This orbital-free description is shown to be consistent with an incipient dissociation of DFD to :CF_2 and N_2 upon excitation. The Laplacian of the electron density and the molecular electrostatic potential exhibit significant reorganization on excitation, mirroring one another, with consequential changes in chemical reactivity. Conforming to Hund's rule, the lowest excited state is a triplet state (T_1), and the next level, the one examined in this work, is the first singlet excited state (S_1) with vertical excitation energies of 2.81 and 3.99 eV, respectively. The calculated dipole moment magnitudes (in D) are 0.05 (S_0), 0.973 (T_1), and 0.969 (S_1) all pointing their negative end toward the nitrogens. The maximal average lifetime of S_1 (in absence of non-radiative de-excitation) is ca. 30 ps, sufficient for its slowest vibrational normal mode to complete 400 oscillations. From a comparison of Hartree–Fock, MP2, QCISD, CCSD, and TD-DFT/B3LYP calculations with experiment (all using an aug-cc-pVTZ basis set), for both the ground and excited states of DFD, the method of choice appears to be QCISD, the one used in this work.

Keywords 3,3′-Difluorodiazirine (DFD, CF_2N_2) · Dipole moment of the excited state · Electrostatic potential of the excited state · Laplacian of the electron density of the excited state · Quantum theory of atoms in molecules (QTAIM) in excited states

Published as part of the special collection of articles "CHITEL 2015 - Torino - Italy".

✉ Chérif F. Matta
cherif.matta@msvu.ca

[1] Departamento de Química e Física Molecular, Instituto de Química de São Carlos, Universidade de São Paulo, Av. Trabalhador São-Carlense, 400 – CP 780, São Carlos, SP 13560-970, Brazil

[2] Department of Chemistry and Physics, Mount Saint Vincent University, Halifax, NS B3M 2J6, Canada

[3] Department of Chemistry, Dalhousie University, Halifax, NS B3H 4J3, Canada

[4] Department of Chemistry, Saint Mary's University, Halifax, NS B3H 3C3, Canada

1 Introduction

The difluorocarbene radical (:CF_2) is widely used in stereospecific organic synthesis [1, 2] and in the photoaffinity labeling of biological macromolecules [3]. An experimental route to generate this radical in solution is through the pyrolytic or (flash) photolytic decomposition of 3,3-difluorodiazirine (CF_2N_2), also known as perfluorodiazirine [1, 2, 4]:

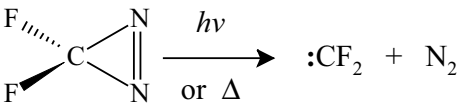

(1)

The photo (or thermally)-induced generation of :CF_2 from 3,3′-difluorodiazirine via reaction (1) has been proposed as a synthetic method to obtain substituted perfluorocyclopropanes by simple addition of the radical to olefins [1, 2]. Recently, due to their photoreactivity and small size, diazirines have also been used as photoreactive labeling agents in studies of ligand–receptor, enzyme–ligand, protein–protein, and protein–nucleic acids interactions by introducing targeted covalent ligands as cross-linkers, fluorophores, or spin labels [3]. The facile generation of difluorocarbene radicals from reaction (1) and their aforementioned usefulness prompted several workers to design synthetic routes for its precursor, namely, 3,3′-difluorodiazirine [1, 2, 5, 6].

In analogy to unsubstituted diazomethane (CH_2N_2) [7], there can be seven different isomers of difluorodiazomethane (CF_2N_2), which are displayed in Fig. 1. To date, only two of those seven possible isomers have been observed experimentally [4, 8–10], namely difluorodiazomethane $F_2C{=}N^+{=}N^-$, and difluorodiazirine $F_2\overline{C-N{=}N}$ (3,3′-difluorodiazirine, or DFD) with a strained three-membered CNN ring (Fig. 2).

The geometry of the S_0 electronic ground state of DFD has been investigated by traditional infrared (IR) spectroscopy [4], high-resolution rotationally resolved Fourier transform-IR spectroscopy [10], Raman spectroscopy [4, 9], gas-phase electron diffraction [8], and high levels of ab initio quantum chemical theory [11]. The geometry of the S_1 first singlet electronic excited state of difluorodiazirine has been inferred from microwave spectroscopic rotational centrifugal distortion constants [12].

The transition from the ground state to the first singlet excited state of DFD is an $n\pi^*$ promotion of an n (nonbonding) electron from nitrogen to the N=N π^* orbital [13]. This transition is denoted as $\tilde{A}^1B_1 \leftarrow \tilde{X}^1A_1$ when the molecular axes are labeled as in Fig. 2 [14, 15], a convention adopted in this work. (Note that Lombardi et al. denote this transition as $\tilde{A}^1B_2 \leftarrow \tilde{X}^1A_1$ in their convention as they switch the x- and y-axes [13, 14].)

As shown in Fig. 2, DFD is a cyclic compound with C_{2v} point group symmetry consisting of a central carbon bonded to two nitrogen atoms and two fluorine atoms. Given this symmetry and the different electronegativities of N and F atoms, respectively, 3.0 and 4.0 (Pauling scale) [16], one predicts a net flow of electronic charge from the diazo group (–N=N–) to the two terminal fluorine atoms via the intervening carbon atom. Since carbon is the element with the lowest electronegativity in this molecule (2.5) [16], it is predicted that this atom will be the most depleted from electronic charge, with more of its charge being withdrawn by the two fluorine atoms and to a lesser extent by the diazo group. Our results, discussed in more details below, are aligned with these qualitative predictions.

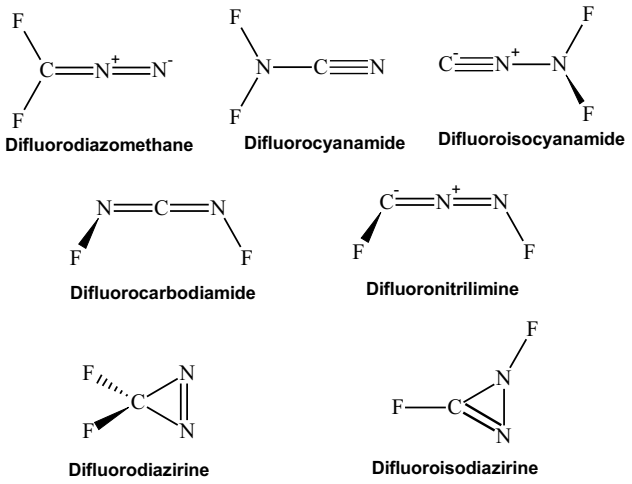

Fig. 1 Structural isomers of CF_2N_2

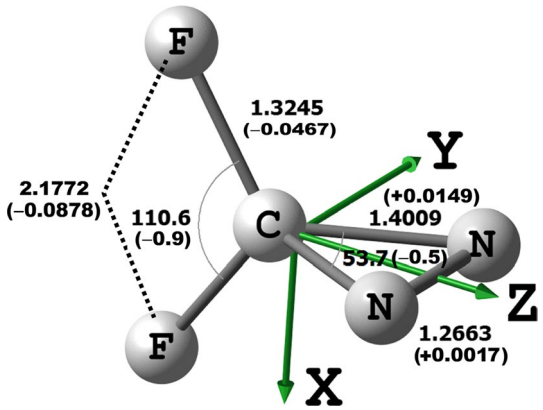

Fig. 2 A ball-and-stick model of the optimized geometry of the ground state of difluorodiazirine (CF_2N_2) calculated at the QCISD/aug-cc-pVTZ level of theory along with the right-handed Cartesian coordinate axis used in this work. Distances are in angstrom (Å) and angles (a–b–c) are in degrees (°). The signed values in parentheses represent the changes in the geometric parameters upon excitation to the first singlet excited state (a positive value means that the parameter has a larger magnitude in the excited state). The excited-state geometry optimizations were performed at the UQCISD/aug-cc-pVTZ level of theory. Also see Table 2

Thus, the charges $q(\Omega)$ (of atom Ω) for the ground state at the quadratic configuration interaction with single and double excitations [17] (QCISD)/aug-cc-pVTZ level of theory followed by quantum theory of atoms in molecules (QTAIM) [18–20] atomic integrations are, in atomic units (a.u.), $q(C) = +1.99$, $q(N) = -0.29$, and $q(F) = -0.70$.

A point-charge model based on these atomic charges whereby atomic charges are placed at the nuclear positions, yields a net dipole moment of approximately 0.33 eÅ = 1.60 debye (D) parallel to the C_2 axis pointing in the positive z-direction in the "physicist convention" [21, 22]. That is, the negative pole of the dipole points to the

side of the two fluorine atoms (negative z-axis) and the positive pole to the side of the –N=N– moiety (positive z-axis). This would have been a significant dipole moment in the ground electronic state S_0 of DFD that could have been experimentally detected, say, by microwave rotational spectroscopy. Instead, the ground state of DFD has long been known to possess such a small dipole moment that its microwave spectrum cannot be observed experimentally [14] and is listed as zero in Table 5.8 (p. 133) of Ref. [23].

According to Hund's rule, the state resulting from the electronic configuration with the highest multiplicity is usually the lowest in energy. Our (U)QCISD/aug-cc-pVTZ vertical excitation energies predict that the first excited state is indeed a triplet state (T_1) followed by the first singlet excited state (S_1), the latter being the state analyzed in this work. The vertical excitation energies are found to be 2.810 eV (T_1) and 3.987 eV (S_1).

The first singlet excited state of DFD, S_1, has the same point group symmetry as its ground state (C_{2v}) as demonstrated by ultraviolet (UV) spectroscopy [24]. However, in contrast to the zero-dipole moment of the ground state, a dipole moment of 1.5 D is listed for the S_1 first singlet excited state in Table 5.8 (page 133) of Turro's monograph [23] (the citation to the primary literature [25] in this monograph appears to be erroneous). Microwave spectroscopy data obtained by Lombardi et al. [13] yielded 1.5 ± 0.2 D for the dipole moment magnitude in the first singlet excited state, consistent with the value listed in Turro's monograph.

Early self-consistent field molecular orbital (SCF-MO) calculations (Hartree–Fock) with a double-zeta basis set performed by Lombardi et al. [13] reveal that this vector is oriented such that its *positive* pole is at the side of the fluorine atoms while its *negative* end is at the side of the nitrogens. This direction of the dipole moment vector is opposite to a simple point-charge model whether in the ground state or in the excited state. Our own calculations at several levels of electronic structure theory, discussed below, agree with the experimental values of the dipole magnitude and its direction inferred by the calculations of Lombardi et al. [13].

For the S_1 excited state of DFD at the geometry of the ground state, our QTAIM atomic charges at the unrestricted QCISD (UQCISD/aug-cc-pVTZ) level of theory are (in a.u.): $q(\mathrm{C}) = +2.25$, $q(\mathrm{N}) = -0.38$, and $q(\mathrm{F}) = -0.74$. A point-charge model based on these atomic charges yields a net dipole moment of 0.68 D parallel to the C_2 axis pointing in the positive z-direction. This simple model yields a dipole moment directed opposite to both experiment and theory, that is, pointing its positive end toward the –N=N– moiety and the negative end toward the fluorine atoms (exptl. 1.5 ± 0.2 D [13], calc. 0.97 D, both pointing in the negative z-direction).

These observations demand an explanation. Questions that emerge from the above discussion may include: (1) Why is the ground-state dipole moment almost null despite of significant electronegativity differences mirrored by the calculated charge transfers? (2) How come the excited state exhibits a dipole moment that points its *negative* end to the lesser electronegative atoms (nitrogens) rather than to the side of the most electronegative ones (fluorines)? (3) Can a study of the electron density and electrostatic potential (ESP) and their changes upon excitation shed some light on the photoreactivity of DFD?

This work will address these questions through an analysis of the changes in the electron density distribution and in the ESP upon electronic excitation (the transition $\tilde{A}^1B_1 \leftarrow \tilde{X}^1A_1$). The atomic and bond properties of diazirine in its ground and lowest excited singlet state will be analyzed within the framework of QTAIM [18–20]. This contributes to the emerging field of the topological analysis of the electron density in the excited state following the lead of earlier studies by Bader [26] and by others [27–31].

2 Molecular dipole moment as a sum of atomic contributions

QTAIM has been the subject of numerous and exhaustive reviews and will not be described here. Only a few salient points on the manner in which this theory decomposes (or reconstructs) the molecular dipole moment to (or from) atomic and/or group contributions are briefly outlined.

QTAIM decomposition/reconstruction of the molecular dipole moment differs in significant ways from its decomposition in terms of additive bond dipole moment vectors as described, for example, in Refs. [32, 33]. QTAIM defines a different type of "bond dipole moment" (that will *not* yield the molecular dipole moment upon vector addition), termed the "charge transfer dipole", arising from the flow of electronic charge across the interatomic zero-flux surface from one atom to a neighboring bonded atom. The charge transfer dipolar contribution must be supplemented by a second one, the atomic dipolar polarization, to recover the molecular dipole moment. That latter contribution arises from the departure of an atom in a molecule from spherical symmetry giving rise to a spatial non-coincidence of the centers of electronic and nuclear charge.

Moving the arbitrary molecular origin of the coordinate system to the position of the nucleus of atom Ω (repeating for every Ω in the molecule) transforms the position vector $\mathbf{r}$ to:

$$\mathbf{r}_\Omega = \mathbf{r} - \mathbf{R}_\Omega, \tag{2}$$

which allows us to re-express the molecular or multi-atomic group dipole moment ($\boldsymbol{\mu}$) as a sum of atomic terms [18, 34–38]:

$$\boldsymbol{\mu} = \sum_{\Omega} \left[-\int_{\Omega} \mathbf{r}_{\Omega} \rho(\mathbf{r}) d\mathbf{r} + \left(Z_{\Omega} - \int_{\Omega} \rho(\mathbf{r}) d\mathbf{r} \right) \mathbf{R}_{\Omega} \right], \quad (3)$$

where ρ is the electron density, Z_{Ω} is the atomic number (which equals the nuclear charge in a.u.), $\mathbf{R}_{\Omega}$ is the position vector of the nucleus of atom Ω in the molecular frame, and the sum runs over all atoms in the molecule or the multi-atomic group.

The last integral in Eq. (3), that of the electron density over an atomic basin, yields the atomic electron population denoted by $N(\Omega)$. Realizing that the atomic charge ($q(\Omega)$) is defined as the difference ($Z_{\Omega} - N(\Omega)$), we can rewrite this equation as:

$$\boldsymbol{\mu} = \sum_{\Omega} \left[\underbrace{\boldsymbol{\mu}_{\mathrm{AP}}(\Omega)}_{\substack{\text{atomic dipolar} \\ \text{polarization}}} + \underbrace{q(\Omega)\mathbf{R}_{\Omega}}_{\substack{\text{charge transfer} \\ \text{dipolar} \\ \text{polarization}}} \right] \equiv \sum_{\Omega} \boldsymbol{\mu}(\Omega), \quad (4)$$

where the molecular dipole $\boldsymbol{\mu}$ is written as a sum of atomic terms, $\boldsymbol{\mu}(\Omega)$. Every atomic term is the sum of an "atomic dipolar polarization" contribution, $\boldsymbol{\mu}_{\mathrm{AP}}(\Omega)$, and a "charge transfer dipolar" (or "bond dipole") contribution, $\boldsymbol{\mu}_{\mathrm{CT}}(\Omega) = q(\Omega)\mathbf{R}_{\Omega}$. Provided the molecule or group is electrically neutral, the sum in Eq. (4) always yields the origin-independent molecular dipole moment $\boldsymbol{\mu}$ despite of consisting of a sum that includes origin-dependent terms.

The transformation in Eq. (2), $\mathbf{r}_{\Omega} = \mathbf{r} - \mathbf{R}_{\Omega}$, places the origin of each $\boldsymbol{\mu}_{\mathrm{AP}}(\Omega)$ at the atomic nucleus lifting its dependence on the origin of the molecular coordinate system. However, the charge transfer term as written in Eq. (4) clearly depends on the origin of the molecular coordinate system through its explicit dependence on the nuclear positions $\mathbf{R}_{\Omega}$. It follows, then, that Eq. (4) represents an infinite number of exact equations, one for each of the infinite number of possible origins.

Realizing that the charge of an atom is equal to the negative of the net flux in electronic charge through its bounding zero-flux surface, we can write:

$$q(\Omega) = -\sum_{\Omega' \neq \Omega} q(\Omega'), \quad (5)$$

where Ω' are neighboring atomic basins that each share a bond path and an associated zero-flux interatomic surface with Ω (all Ω' are taken to be disconnected, i.e., not part of a closed circuit of bonds such as a ring or a cage).

The origin-dependent ambiguity of the charge transfer term can now be resolved by the transformation:

$$\mathbf{r}_{\Omega|\Omega'} = \mathbf{R}_{\mathrm{BCP}}(\Omega|\Omega') - \mathbf{R}_{\Omega}, \quad (6)$$

which re-expresses the position vector of the bond critical point (BCP) associated with interatomic surface $S(\Omega|\Omega')$, $\mathbf{r}_{\Omega|\Omega'}$, in the local (atomic) coordinate system [26, 34, 35]. In this transformation, $\mathbf{R}_{\mathrm{BCP}}(\Omega|\Omega')$ is the position vector (in the molecular coordinate system) of the bond critical point (BCP) between atoms Ω and Ω' at the intersection of the bond path linking them and the zero-flux interatomic surface $S(\Omega|\Omega')$ separating them.

With this second transformation the molecular dipole moment $\boldsymbol{\mu}$ can now be written as a sum of unique, well-defined, additive atomic contributions, i.e., in terms of a sum of the members of the set $\{\boldsymbol{\mu}(\Omega)\}$ [34]:

$$\begin{aligned} \boldsymbol{\mu} &= \sum_{\Omega} \boldsymbol{\mu}(\Omega) \\ &= \sum_{\Omega} \left\{ \boldsymbol{\mu}_{\mathrm{AP}}(\Omega) + \sum_{\Omega' \neq \Omega} q(\Omega') \left[\mathbf{R}_{\mathrm{BCP}}(\Omega|\Omega') - \mathbf{R}_{\Omega} \right] \right\}, \end{aligned} \quad (7)$$

where

$$\boldsymbol{\mu}(\Omega) = \boldsymbol{\mu}_{\mathrm{AP}}(\Omega) + \boldsymbol{\mu}_{\mathrm{CT}}(\Omega), \quad (8)$$

$$\boldsymbol{\mu}_{\mathrm{AP}}(\Omega) = -\int_{\Omega} \mathbf{r}_{\Omega} \rho(\mathbf{r}) d\mathbf{r}, \quad (9)$$

$$\boldsymbol{\mu}_{\mathrm{CT}}(\Omega) = \sum_{\Omega' \neq \Omega} q(\Omega') \left[\mathbf{R}_{\mathrm{BCP}}(\Omega|\Omega') - \mathbf{R}_{\Omega} \right]. \quad (10)$$

Keith has generalized these considerations to a wider set of properties termed "null properties," which include the dipole moment, dipole moment derivatives, and atomic energies and presented solutions to the problem of atoms that partake in rings and/or cages [39]. As noted by Keith, the charge transferred between atoms which partake into a cyclical closed structure such as a ring or a cage is generally ill-defined. A notable exception to this ill-definition is when symmetry dictates an equal sharing of electronic charge across symmetry-equivalent interatomic surfaces within the cyclical structure. Difluorodiazirine falls into this latter category whereby the charge flux through a $S(\mathrm{C|N})$ zero-flux interatomic surface is well defined since the two nitrogen atoms are equivalent by symmetry, each carrying an identical charge. Hence, we will omit the discussion of Keith's (important) generalization of the above treatment to cyclical structures since it falls outside of the scope of the present work.

3 Computational methods

To simplify the interpretation of results, calculations were done with different ab initio electronic structure methods but in conjunction with one and the same basis set. This basis set is aug-cc-pVTZ, a large correlation-consistent

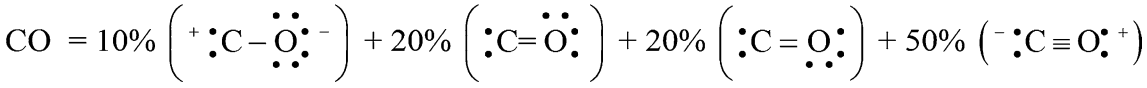

Scheme 1 Pauling's contributing resonance structures to the ground state of CO

Dunning triple-zeta basis set augmented with the diffuse functions necessary for the correct description of electronic excited states [40]. Calculations were done within the frameworks of Hartree–Fock [HF, or self-consistent field (SCF)] theory [41], second-order Møller–Plesset perturbation theory (MP2) [42], coupled cluster theory with single and double excitations (CCSD) [43–45], quadratic configuration interaction with single and double excitations (QCISD) [17], and density functional theory [46, 47] (Becke [48] and Lee–Yang–Parr [49] hybrid functional, B3LYP). Post-SCF calculations (MP2, CCSD, and QCISD) were done with the frozen core (FC) approximation.

Excited states were calculated using the restricted open-shell (RO) and the unrestricted (U) formulations of HF/aug-cc-pVTZ, MP2/aug-cc-pVTZ, CCSD/aug-cc-pVTZ, QCISD/aug-cc-pVTZ, and B3LYP/aug-cc-pVTZ. The unrestricted formulation has been significantly superior in recovering studied experimental properties, and hence, in this paper, only the results quoted are exclusively those obtained with the unrestricted formulation unless mentioned otherwise.

Since the available experimental values are better reproduced by the levels of theory denoted QCISD/aug-cc-pVTZ and UQCISD/aug-cc-pVTZ for the ground and excited states, respectively, results that are also very close to the corresponding ones from CCSD calculations, the QCISD values are the ones upon which the discussion is based unless stated otherwise. Results at the other levels of theory are not tabulated in as much detail since *trends* in molecular and QTAIM properties in all discussed quantities are unchanged. This level of theory insensitivity of QTAIM properties is well documented [50–52].

At each level of theory, the molecular geometry of the ground state was optimized by minimizing the energy gradients to within 2×10^{-6} and 1×10^{-6} hartree/bohr [atomic units (a.u.)] for the residual maximum force and the root mean square (RMS) force on the nuclei, respectively. Frequency calculations confirmed that the structure was a true minimum at each level of theory.

Two singlet $\tilde{A}^1B_1$ excited-state calculations were performed: (1) vertically excited-state calculation at the frozen optimized geometry of the ground state as required by the Frank–Condon principle and (2) adiabatically excited state calculation whereby the geometry of the excited state has been gradient optimized with the same convergence thresholds described above.

All electronic structure calculations, geometry optimizations, vibrational frequency determinations, and generation of wave functions and electron density and electrostatic potential three-dimensional grids were conducted using Gaussian 09 [53]. Wave functions and electron densities were analyzed with AIMAll/AIMStudio [54] to generate the QTAIM properties. In no case, the magnitude of the atomic Lagrangian exceeds 5.16×10^{-4} a.u., which indicates high integration precision. The differences between the sums of atomic populations and the total number of electrons ($N = 38\ e^-$) are tiny and remain around $10^{-7}\ e$ for the ground and excited states. The differences between the sums of atomic (virial) energies and the total energies (in kcal/mol) are -0.04 and -0.27, for the ground and adiabatically excited states, respectively. The UQCISD singlet excited-state calculations (both vertical and adiabatic) result in $\langle S^2 \rangle$ which is equal to $s(s+1)$ to four decimals (0.0000), indicating no spin contamination.

4 Results and discussion

4.1 Preliminary observations

QTAIM has already been used to elucidate the atomic origins of molecular dipole moments, which was particularly illuminating in cases where the observed dipole is inconsistent with expectation based on electronegativities. A well-known case of an anomalous dipole moment is that of the carbon monoxide molecule, CO. This molecule has a very small dipole moment in its ground state with a polarity opposite to the one expected from electronegativity differences, symbolized by: $^-\overrightarrow{C = O}^+$ [16, 18, 55–57].

Pauling explained this anomaly by fitting the percentage weights of various resonance structures (on the basis of bond lengths) to the observed equilibrium bond length of this molecule [16]. We express Pauling's proposal schematically in Scheme 1.

The dominance of the last resonance structure in Scheme 1 is how Pauling reconciles his resonance model with the observed experimental dipole moment.

Frenking et al. [55] explain the anomaly by decomposing the molecular dipole moment into molecular orbital (MO) contributions. These workers note that the highest occupied MO (HOMO), which has σ-symmetry, is localized primarily over the carbon atom (the carbon lone pair), while the oxygen lone pair is dominated by *s*-type

Scheme 2 QTAIM atomic decomposition/reconstruction of the dipole moment of CO

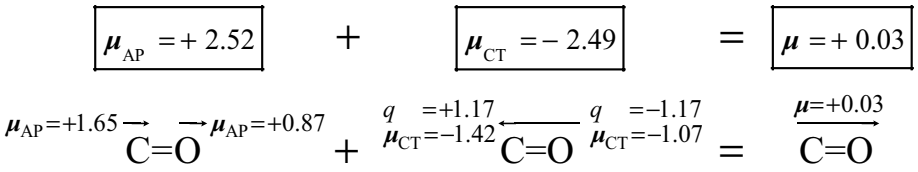

Table 1 Calculated vibrational frequencies of difluorodiazirine (CF_2N_2) for the ground and excited states (S_0 and S_1) along with the experimental values for S_0

Symmetry	S_0					S_1
	MP2	QCISD	CCSD	B3LYP	Exptl.[a]	UQCISD[c]
A_2	429	443	443	437	448	431
B_1	460	471	471	467	481	461
A_1	477	489	488	480	502	488
B_2	527	540	538	522	544	495
A_1	777	799	798	785	805	836
B_2	1071	1102	1100	1059	1091	985
B_1	1174	1251	1252	1189	1248	1392
A_1	1208	1306	1307	1268	1282	1476
A_1	1473	1592	1590	1587	1563	1596
Av.|dev.| ± std[b]	41 ± 28	12 ± 9	12 ± 8	24 ± 14		

Calculations were done with the indicated electronic structure methods all in conjunction with a aug-cc-pVTZ basis set. Vibrational frequencies are expressed in wave numbers in units of cm^{-1}

Vibrational frequencies are all scaled to empirically correct for anharmonicity of the normal modes. Scaling parameters used (±std) are [66]: MP2: 0.953 ± 0.033, QCISD: 0.962 ± 0.017, CCSD: 0.956 ± 0.017, and B3LYP: 0.968 ± 0.019

[a] Taken from Ref. [4]

[b] Average absolute deviations from the experimental value (Av.|dev.|) ± standard deviation (std) for the ground state, S_0, taken over all nine frequencies

[c] Predicted excited state scaled vibrational frequencies. These may be observed provided the lifetime of a fraction of the population of molecules in the excited state survives for at least one vibration (the period of the slowest vibration, that with wave number = 431 cm^{-1}, ≈77.4 fs, while that of the fastest is 1596 cm^{-1} ≈ 20.9 fs). See text

contributions and is non-contributing to the dipole moment due to its spherical symmetry [55].

An alternative real-space explanation was provided by Bader [18, 57] whereby the dipole moment of CO is shown to result from (a) a charge transfer dipole, which conforms with expectations in its direction, and (b) an atomic polarization dipole that results from the non-sphericity of atomic electron densities. The latter dipole is opposite in direction to the former and slightly exceeds it in magnitude leading to the observed dipole moment of CO (see Scheme 2).

We briefly recap the QTAIM explanation of the dipole anomaly of CO. The atomic charges are (in a.u.) $q(C) = +1.17$ and $q(O) = -1.17$, leading to a charge transfer (CT) dipole of $\boldsymbol{\mu}_{CT}(C) + \boldsymbol{\mu}_{CT}(O) = -1.42–1.07 = -2.49$ a.u. (second term in Scheme 2, in the physicist convention with the coordinate axis directed from C to O). The charge transfer dipole is negative as expected from electronegativity considerations. The opposing atomic dipolar polarization is $\boldsymbol{\mu}_{AP}(C) + \boldsymbol{\mu}_{AP}(O) = 1.65 + 0.87 = +2.52$ a.u. (first term in Scheme 2). The sum, $\boldsymbol{\mu}_{CT}(CO) + \boldsymbol{\mu}_{AP}(CO) = -2.49 + 2.52 = 0.03$ a.u. (~0.08 D), a small dipole moment pointing its *negative* end toward the carbon atom, as experimentally observed.

This explanation has the advantage over the resonance or the MO models in that it is entirely based on a topological analysis of the total molecular charge distribution, a quantum mechanical observable in the sense of Dirac [58, 59] that is experimentally measurable by high-resolution X-ray diffraction [60–62].

Before performing a similar decomposition/reconstruction of the dipole moment of difluorodiazirine in both its ground and excited electronic states, we first assess the quality of the prediction of a number of molecular properties of this molecule by various model chemistries. Some spectroscopic properties (IR and UV) are explored first followed by a comparison of molecular geometries and their changes in the excited state with experiment.

4.2 Vibrational frequencies

There are $3n - 6 = 9$ vibrational normal modes for a penta-atomic molecule such as difluorodiazirine. Table 1 lists the symmetries of these vibrations along with the scaled harmonic frequencies for the ground state of difluorodiazirine calculated using four model chemistries (the scaling accounts empirically for vibrational anharmonicity). The table also presents the experimental frequencies and the average absolute deviation (±standard deviation) from the experimentally determined frequencies of the ground state for each model chemistry. The goodness of the agreement with the experimentally determined ground-state vibrational frequencies is ordered as follows: QCISD ≈ CCSD > B3LYP > MP2. The average error (±STD) of the best (QCISD) results is 11.8(8.7) cm^{-1}.

Given the superior ability of QCISD in recovering experimental frequencies for the ground state (in addition to its ability to accurately predict the set of properties discussed below), it is the method chosen to calculate the frequencies of the excited state as well, which are given in Table 1. The excited-state vibrational spectrum has never been recorded experimentally, probably because of its extremely short lifetime as the estimates below indicate. All but two frequencies change significantly in the excited state (by 10 cm^{-1} or more). The frequency that experiences the largest bathochromic shift (of −117 cm^{-1}) is predicted to be the sixth (of B_2 symmetry), while the one exhibiting the largest hypsochromic shift (of +170 cm^{-1}) in the excited state is the penultimate frequency (of A_1 symmetry).

The maximum average lifetime, τ_{rad}, of the excited state from spontaneous radiative decay (in absence of any other deactivating or quenching mechanisms) can be predicted from Einstein coefficient A_{10} [63]:

$$A_{10} = \frac{1}{\tau_{rad}} = \frac{8\pi^2 e^2 \omega^2}{(4\pi\varepsilon_0) c m_e} f, \tag{11}$$

where m_e and e are the mass and the magnitude of the charge of the electron, respectively, c is the speed of light in vacuum, ω is the reciprocal wavelength of the absorbed photon, f is the (dimensionless) oscillator strength, and the remaining of the symbols have their usual meaning.

The calculated oscillator strength (the length form) for the vertical $S_1 \leftarrow S_0$ transition is $f = 0.0040$ (QCISD), 0.0040 (CCSD), 0.0039 (MP2), and 0.0016 (TD-B3LYP). Based on a value of $f = 0.004$, τ_{rad} is predicted to lie in the vicinity of 30 ps. (The calculated oscillator strength of the spin-forbidden transition to the lowest excited state, $T_1 \leftarrow S_0$, is zero to four decimals, but our calculations do not include any vibronic coupling.)

From Table 1, the slowest vibration in the excited state has a wave number of 431 cm^{-1} which is equivalent to a period of approximately 77.4 fs, and hence can complete ca. 388 oscillations within $\tau_{rad} = 30$ ps. These considerations suggest that all normal modes necessary for the generation of a full IR spectrum of the excited state, as listed in Table 1, can be observable within τ_{rad} provided the excited state's lifetime is not severely reduced (by two orders of magnitude) by other reactive and/or non-radiative de-excitation mechanisms.

4.3 Electronic excitation energies

Table 2 lists both the adiabatic and vertical excitation energies in comparison with reliable reference data. The reference value for the adiabatic transition, ΔE_{ad}, was calculated by Hoffmann et al. [11] at the GVVPT2/cc-pVTZ level of theory and is 2.86 electron volts (eV) (ΔE_{ad} increases slightly to 3.04 when a smaller basis set such as cc-pVDZ is used).

The second half of Table 2 shows the calculated vertical excitation energies without the ZPE correction (E_{ZPE}), entries denoted as $\Delta E_{vert(raw)}$, and those obtained after the addition of the ground-state ZPE correction to derive the corrected vertical excitation energy, $\Delta E_{vert(corr)} = \Delta E_{vert(raw)} + E_{ZPE}$. The $\Delta E_{vert(corr)}$ are the values to be compared with the experimental one (3.52 eV, taken from Hollas et al. [14]), as required by the Franck–Condon principle.

A comparison of the results obtained with the tested theoretical models indicates that for vertical and adiabatic excitations, the excitation energy is overestimated by about 0.8–0.9 eV for most methods (with around 30 % discrepancy from the reference values), with B3LYP exhibiting the smallest difference from the reference value. This is the only studied property where B3LYP outperforms other methods. The most trustworthy methods (QCISD and CCSD) give similar results, with the former being the only method that gives the same relaxation energy (energy difference between the reference adiabatic and vertical excitation energies): Ref. (3.52–2.86 = 0.66 eV) = UQCISD (4.44–3.78 = 0.66 eV). Since generally unrestricted and restricted open-shell calculations give similar results, and since UQCISD appears as a candidate method of choice to treat the ground and excited states on equal footing, and for consistency and simplicity of the discussion, *only the unrestricted formulations (U) of the electronic structure methods will be examined in the following and the distinction between RO and U becomes unnecessary from now on unless stated otherwise explicitly*.

4.4 Geometries of the ground and excited states

The geometries of the ground and excited states of difluorodiazirine obtained from unconstrained energy gradient optimizations at the various levels of theory are summarized in Table 3. The table also compares the calculated and available experimental geometrical parameters [8, 13].

Table 2 Excitation energy of difluorodiazirine (CF_2N_2) calculated with different standard electronic structure methods, all using an aug-cc-pVTZ basis set

Method[a]	Adiabatic[b]		$\Delta E_{\text{vert(raw)}}$	E_{ZPE}	Vertical[b]	
	ΔE_{ad}	Dev.[c]			$\Delta E_{\text{vert(corr)}} = \Delta E + E_{\text{ZPE}}$	Dev.[c]
HF (RO)	3.50	0.64	4.00	0.48	4.48	0.96
MP2 (RO)	3.69	0.83	3.90			
MP2 (U)	3.78	0.92	3.90			
QCISD (RO)	3.69	0.83	3.99	0.45	4.44	0.92
QCISD (U)	3.78	0.92	3.99	0.45	4.44	0.92
CCSD (RO)	3.69	0.83	3.99	0.46	4.45	0.93
CCSD (U)	3.69	0.83	3.99	0.45	4.44	0.92
DFT/B3LYP (RO)	3.14	0.28	3.47	0.44	3.91	0.39
DFT/B3LYP (U)	3.17	0.31	3.47	0.50	3.97	0.45
Reference[d,e]	2.86 [11]				3.52 [14]	

All energies entered in the table are in electron volts (eV)

[a] RO = restricted open shell for the excited-state calculation; U = unrestricted open shell for the excited state calculation. UHF could not be converged to a stable solution in either the vertical or adiabatic excited state. Also, both ROMP2 and UMP2 calculations for the vertically excited state did not converge

[b] Calculated adiabatic energy differences (ΔE_{ad}) do not include zero-point vibrational energy (ZPE) corrections (*i.e.*, bottom-of-the-well differences). Vertical excitation energies (ΔE_{vert}) are obtained by differences using the excited-state total energy calculated at the optimized geometry of the ground state. Thus, in accordance with the Frank–Condon principle, and for a direct comparison with experiment, the ZPE correction is included for the ground state only when calculating the vertical excitation energies

[c] Deviation (dev) is defined as the calculated value minus the reference value

[d] The reference value for the adiabatic excitation energies is obtained from high level ab initio calculations at the GVVPT2/cc-pVTZ level by Hoffmann et al. [11] (and becomes 3.04 with a smaller basis set at the level of theory denoted by GVVPT2/cc-pVDZ) [11]. These reference values were calculated in the same manner as the adiabatic energies in this work, that is, without the inclusion of ZPE corrections

[e] The experimental reference value for vertical energies is compared with the sum $\Delta E + E_{\text{ZPE}}$

MP2 agrees best with experiment for the ground state, as can be seen by the difference between geometrical parameters from the various methods and experimental values [8]. The average absolute deviations for interatomic distances (in Å) are in increasing order: MP2 (0.011) < CCSD (0.015) < QCISD (0.016) < DFT/B3LYP (0.022) < HF (0.043). The respective order found for the interatomic angles (in degrees) is: MP2 (0.8) < QCISD (1.7) = CCSD (1.7) < DFT/B3LYP (1.9) < HF (2.7). Both QCISD and CCSD appear reasonable in the prediction of both interatomic distances and angles, following MP2 closely in this aspect.

The average deviations over the only two observed experimental parameters for the excited state (N–N and F–F distances) are in increasing order: B3LYP (0.019) < CCSD = MP2 = QCISD (0.065). In this respect, QCISD and CCSD appear to reasonably follow experimental trends.

Finally, the trends in the excitation-induced *change* in the two experimental interatomic distances are examined. The increasing order of the average in the absolute deviation from experiment is: B3LYP (0.004) < CCSD (0.025) < QCISD (0.026) < MP2 (0.035). The trends in the geometrical parameters are consistent and both QCISD and CCSD appear sufficiently accurate in recovering the geometries and their changes in going from the ground to the excited state of difluorodiazirine.

4.5 Charge distribution in the ground and excited states

The calculated and experimental dipole moments of difluorodiazirine, for both the ground and excited states, are given in Table 4 (under the column labeled as $\boldsymbol{\mu}$). The dipole moments calculated by the electronic structure methods investigated here are identical in their direction and almost identical in magnitude to one decimal place. Hence, all methods give a dipole moment between −0.0 and 0.1 D for the ground state, which is consistent with the lack of its experimental detection [14, 23]. For the excited state, all methods agree closely giving a dipole of 1.0 D, comparable with the experimental magnitude of 1.5 ± 0.2 D [23, 24]. Therefore, the electronic structure methods analyzed in Table 4 are capable of predicting the dipole moment of

Table 3 Calculated (and experimental) geometrical parameters for the ground and first singlet excited state of difluorodiazirine (CF_2N_2) obtained with different standard electronic structure methods (with unrestricted formulations for the excited state), all using an aug-cc-pVTZ basis set (see Fig. 2)

Method	*d*(F–C)	*d*(N–N)	*d*(N–C)	*d*(F–F)	ΣAD[a]	N–C–N	F–C–F	F–C–N
Ground state (S_0)								
HF	1.306	1.223	1.374	2.137		52.87	109.87	120.96
	0.009	0.070	0.052	0.041	0.173	2.08	1.97	4.05
MP2	1.328	1.295	1.405	2.185		54.88	110.68	120.31
	−0.013	−0.002	0.021	−0.007	0.043	0.07	1.16	1.22
QCISD	1.325	1.266	1.401	2.177		53.74	110.55	120.54
	−0.010	0.027	0.025	0.001	0.062	1.21	1.29	2.50
CCSD	1.323	1.265	1.407	2.175		53.68	110.62	120.52
	−0.008	0.028	0.019	0.003	0.058	1.27	1.23	2.49
B3LYP	1.333	1.259	1.405	2.192		53.26	110.65	120.57
	−0.018	0.034	0.021	−0.014	0.087	1.69	1.19	2.88
Exptl. [8]	1.315 (4)	1.293 (9)	1.426 (4)	2.178		54.95 (36)	111.84 (52)	
Excited state (S_1)								
MP2	1.278	1.268	1.416	2.089		53.21	109.69	121.00
		0.075		0.055	0.130			
QCISD	1.278	1.268	1.416	2.089		53.21	109.68	121.00
		0.075		0.055	0.130			
CCSD	1.278	1.268	1.416	2.089		53.21	109.68	120.99
		0.075		0.055	0.130			
B3LYP	1.307	1.309	1.446	2.141		53.83	110.01	120.76
		0.034		0.003	0.037			
Exptl. [13].		1.343		2.144				
Change upon excitation: Param.(S_1) − Param.(S_0)[b]								
MP2	−0.050	−0.027	0.011	−0.095		−1.68	−1.00	0.69
		0.077		0.061	0.138			
QCISD	−0.047	0.002	0.015	−0.088		−0.52	−0.87	0.46
		0.048		0.054	0.102			
CCSD	−0.045	0.003	0.009	−0.086		−0.47	−0.93	0.47
		0.047		0.052	0.099			
B3LYP	−0.026	0.050	0.041	−0.051		0.57	−0.64	0.19
		0.000		0.017	0.017			
Exptl.		0.050		−0.034				

Interatomic atomic distances are in angstrom (Å), and angles (a–b–c) are in degrees (°)

[a] The second line below the entry corresponding to a given level of theory is the difference Δ between the experimental value of the geometric parameter (*P*) and the given calculated value ($\Delta P = P$(Exptl.) − *P*(Calc.)). ΣAD is the sum of the absolute (unsigned) deviations

[b] The change upon excitation $\Delta P_{exc.}$ is defined as: $\Delta P_{exc.} = P$(excited state)—*P*(ground state). When available, the second line below the entry corresponding to a given level of theory is the difference $\Delta\Delta P_{exc.}$ between the experimental value of this change upon excitation and the corresponding signed calculated change ($\Delta\Delta P_{exc.} = \Delta P_{exc.}$(Exptl.) − $\Delta P_{exc.}$ (Calc.))

difluorodiazirine in both electronic states with qualitative and reasonable quantitative agreement with experiment.

Given overall performance, QCISD emerges as a reliable choice for difluorodiazirine and yields results that are analogous to those from CCSD. Hence, *the remainder of this article will refer, discuss and tabulate the results obtained exclusively at the (U)QCISD/aug-cc-pVTZ level unless otherwise stated.*

The questions raised in the introduction are now addressed. The first two questions enquire into *the nature of the electron density distribution that gives rise to the observed vanishing dipole moment in the ground state of difluorodiazirine and its dramatic change upon excitation.* To answer this question, we present the atomic contributions to the ground- and the adiabatically excited-state dipole moments in Table 5. The table only includes data for

Table 4 Calculated and experimental molecular dipole moment ($\boldsymbol{\mu}$) of CF_2N_2 for the ground (S_0) and the first singlet excited state (S_1) together with the atomic polarization contribution ($\boldsymbol{\mu}_{AP}$) and charge transfer contribution ($\boldsymbol{\mu}_{CT}$) to the molecular dipole moment (calculations at the levels of theory defined by the listed electronic structure methods in combination with an aug-cc-pVTZ basis set)

Method	S_0			S_1		
	μ_{AP}	μ_{CT}	μ	μ_{AP}	μ_{CT}	μ
MP2	−1.7612	1.6849	−0.0763	−1.6527	0.6834	−0.9693
QCISD	−1.6390	1.5931	−0.0459	−1.6512	0.6825	−0.9687
CCSD	−1.6347	1.5910	−0.0437	−1.6512	0.6826	−0.9685
B3LYP	−1.6270	1.6135	−0.0135	−2.0353	1.0010	−1.0343
Exptl.			0.0[a]			−1.5 ± 0.2[b]

Dipole moments are in D and oriented according to the physicist convention with respect to the coordinate system displayed in Fig. 2

[a] Experimental values are obtained from Table 5.8 (page 133) of Turro's monograph [23]

[b] Experimental values are obtained from Lombardi et al. [13]

the *adiabatically* excited state since this is the only experimentally accessible excited-state dipole moment.

For the ground state (S_0), the values listed in Tables 4 and 5 indicate that the molecule possesses a very small dipole moment, around 0.05 D in magnitude, pointing to the negative direction of the z-axis of the coordinate system depicted in Fig. 2. In other words, the negative end of the dipole lies at the side of the nitrogen atoms with respect to the xy-plane. All four chemical models are remarkably consistent in this regard as can be seen from the values listed in Table 4.

The vanishingly small dipole moment is the result of two opposing molecular contributions. The first contribution is that of the overall molecular charge transfer dipole, $\boldsymbol{\mu}_{CT} = +1.59$ D, with its negative side toward the fluorine atoms (with respect to the xy-plane), a direction consistent with simple electronegativity arguments. As stated in the introduction, this is the dipole direction expected from a point-charge model using the calculated QTAIM charges listed in Table 5 ($q(\Omega)$). In contrast, what cannot be deduced from a spherical atomic model is the sum of all five atomic polarization terms, $\boldsymbol{\mu}_{AP} = -1.64$ D, which cancels and slightly exceeds the dipole moment that arises from the flow of charge between the atoms by −0.05 D, resulting in the small ground-state molecular dipole moment. As a result of this near vectorial cancelation of the two dipolar contributions, the molecular dipole moment $\boldsymbol{\mu}$ of difluorodiazirine exhibits a magnitude lower than the detection limits of microwave spectroscopy.

The redistribution of electronic charge and the reorganization of the molecular geometry in the excited state (S_1) slightly increases the magnitude of the atomic polarization component (by 0.01 D to reach −1.65 D) but severely reduces the charge transfer dipolar contribution to only 43 % of its initial value in the ground state (+0.68 D). Since the two components of the dipole moment have opposite directions, this decrease in the CT contribution causes the rise in the molecular dipole moment (in the direction of the AP dipole) due to a less effective cancelation of the (now) dominant AP component by the CT dipole.

We are now asked to trace these changes in the two components of the molecular dipole moment to their atomic origins, that is, to seek an answer at an atomic resolution. To answer this question, Table 5 shows the QTAIM atomic contributions to both the overall AP and CT dipolar polarizations for the ground and excited states. Besides the atomic contributions to the AP and CT terms for both electronic states, the table also gives the QTAIM atomic charges ($q(\Omega)$) and the Cartesian coordinates (x, y, z) of the gradient-optimized geometries (that can be used to calculate a nuclei-centered point-charge transfer dipole, as done in Sect. "1"). The last column of the table lists the row sums of the contributions for each type of dipole along each of the three coordinates. This last column of Table 5 corresponds to the row listing the QCISD results in Table 4.

Table 5 has three sections. The first section decomposes the dipole moment of the ground state, the second section decomposes that of the excited state, and the third section lists the *changes* (value for the excited state minus the corresponding value for the ground state) upon adiabatic excitation.

As already mentioned, the most dramatic change upon excitation is that of the CT contribution. An examination of Table 5 shows that total molecular CT contributions vanishes along the x- and the y-axes due to the symmetry despite that the individual atomic contributions are quite significant. For example, the magnitude of the CT dipole for the two fluorine atoms in the x-direction, $|\boldsymbol{\mu}_{CT}(F)_x|$, is 2.47 D in S_0 (which rises to reach a value of 2.61 D in S_1), but these dipoles are oriented in opposite directions for each of the fluorine atoms canceling one another. Similarly, the magnitude of the CT dipole for nitrogen atoms in the y-direction in the ground state ($|\boldsymbol{\mu}_{CT}(N)_y|$) is 0.44 D, a value that becomes 0.69 D in the excited state, and again the dipole moments of the two nitrogen atoms cancel each other by symmetry. Thus, the molecular symmetry dictates an exact cancelation of charge transfer contributions along the x- and y-directions, for both the ground and the excited

Table 5 Atomic decomposition/reconstruction of the molecular dipole moment ($\boldsymbol{\mu}$) of CF_2N_2 for the ground (S_0) and the first singlet excited state (S_1) into interatomic charge transfer contributions ($\boldsymbol{\mu}_{CT}$) and atomic polarization contributions ($\boldsymbol{\mu}_{AP}$) calculated at the (U)QCISD/aug-cc-pVTZ level of theory

Ω	F	F	N	N	C	Sum[a]
S_0						
x	−1.08875	1.08846	0.00029	0.00017	0.00000	
y	−0.00008	0.00012	−0.63330	0.63305	0.00000	
z	−0.75424	−0.75465	1.24964	1.24977	0.00000	
$q(\Omega)$	−0.7005	−0.7005	−0.2901	−0.2901	1.9798	−0.0014
$\boldsymbol{\mu}_{AP}(\Omega)_x$	−0.7951	0.7949	−0.0002	0.0002	−0.0039	−0.0041
$\boldsymbol{\mu}_{AP}(\Omega)_y$	−0.0001	0.0001	1.3686	−1.3686	0.0012	0.0011
$\boldsymbol{\mu}_{AP}(\Omega)_z$	−0.5841	−0.5844	0.0437	0.0434	−0.5575	−1.6390
$\boldsymbol{\mu}_{CT}(\Omega)_x$	2.4714	−2.4708	−0.0002	−0.0002	0.0000	0.0002
$\boldsymbol{\mu}_{CT}(\Omega)_y$	0.0002	−0.0003	0.4350	−0.4345	−0.0002	0.0003
$\boldsymbol{\mu}_{CT}(\Omega)_z$	1.7053	1.7062	−1.0752	−1.0758	0.3312	1.5918
$\boldsymbol{\mu}_z$						−0.0472
S_1						
x	−1.04484	1.04457	0.00029	0.00019	0.00000	
y	0.00023	0.00043	−0.63399	0.63402	0.00000	
z	−0.73562	−0.73601	1.26587	1.26553	0.00000	
$q(\Omega)$	−0.7619	−0.7619	−0.3865	−0.3870	2.2976	0.0002
$\boldsymbol{\mu}_{AP}(\Omega)_x$	−1.0517	1.0515	−0.0000	0.0002	−0.0030	−0.0032
$\boldsymbol{\mu}_{AP}(\Omega)_y$	0.0006	0.0008	1.5222	−1.5211	−0.0006	0.0019
$\boldsymbol{\mu}_{AP}(\Omega)_z$	−0.7318	−0.7322	0.4043	0.4061	−0.9977	−1.6512
$\boldsymbol{\mu}_{CT}(\Omega)_x$	2.6051	−2.6044	−0.0003	−0.0002	−0.0001	0.0001
$\boldsymbol{\mu}_{CT}(\Omega)_y$	−0.0007	−0.0012	0.6944	−0.6956	−0.0013	−0.0043
$\boldsymbol{\mu}_{CT}(\Omega)_z$	1.8251	1.8260	−1.3100	−1.3118	−0.3480	0.6813
$\boldsymbol{\mu}_z$						−0.9699
Change ($\Delta P = P(S_1) - P(S_0)$)[b]						
$\Delta q(\Omega)$	−0.0614	−0.0614	−0.0964	−0.0969	0.3178	0.0016
$\Delta\boldsymbol{\mu}_{AP}(\Omega)_x$	−0.2566	0.2566	0.0001	0.0000	0.0009	0.0010
$\Delta\boldsymbol{\mu}_{AP}(\Omega)_y$	0.0006	0.0007	0.1536	−0.1525	−0.0017	0.0007
$\Delta\boldsymbol{\mu}_{AP}(\Omega)_z$	−0.1477	−0.1477	0.3607	0.3627	−0.4402	−0.0122
$\Delta\boldsymbol{\mu}_{CT}(\Omega)_x$	0.1337	−0.1336	−0.0001	0.0000	−0.0001	−0.0001
$\Delta\boldsymbol{\mu}_{CT}(\Omega)_y$	−0.0008	−0.0009	0.2594	−0.2612	−0.0011	−0.0046
$\Delta\boldsymbol{\mu}_{CT}(\Omega)_z$	0.1198	0.1198	−0.2349	−0.2360	−0.6793	−0.9105
$\Delta\boldsymbol{\mu}_z$						−0.9227

Cartesian coordinates in the table are in angstrom (Å), dipole moments in debye (D), and charges in atomic units (a.u.). Symbols: (x, y, z) are the Cartesian coordinates in the frame depicted in Fig. 2; $q(\Omega)$ is the atomic charge, $\boldsymbol{\mu}_{AP}(\Omega)_i$ is the ith component of the atomic dipolar polarization, $\boldsymbol{\mu}_{CT}(\Omega)_i$ is the ith component of the atomic charge transfer dipolar contribution, $\boldsymbol{\mu}_i$ is the ith component of the molecular dipole moment

[a] The last column lists the rows sums. For the total molecular dipole moment $\boldsymbol{\mu}$, only sums of its z-components are listed since those of the x- and y-components ($\boldsymbol{\mu}_x$, $\boldsymbol{\mu}_y$) vanish by symmetry (with small numerical errors that appear at the third decimal place at most)

[b] Change is defined as the difference between a given parameter (P) in the excited state $P(S_1)$ minus its value in the ground state $P(S_0)$

state, as can be seen from the last column of Table 5 (the small departures from the exact cancelation is due to numerical computational errors).

Now the dipolar polarization along the z-axis is discussed. In the ground state, both fluorine atoms contribute equally to the charge transfer dipole along the z-direction, each contributing $\boldsymbol{\mu}_{CT}(F)_z = +1.71$ D, and both add constructively in the positive z-direction. The CT dipole of the carbon atom in the z-direction also points to the positive z-direction reinforcing the CT dipole contributions of the fluorine atoms, with a CT dipole of $\boldsymbol{\mu}_{CT}(C)_z = +0.33$ D, the total CT dipole of the F_2C group in the positive

z-direction being $\boldsymbol{\mu}_{CT}(F, F, C)_z = +3.74$ D. Meanwhile, the two nitrogen atoms give rise to a combined CT dipole that opposes the net dipole of the F_2C group with a CT dipole of $\boldsymbol{\mu}_{CT}(N)_z = -1.08$ D for each N atom ($\boldsymbol{\mu}_{CT}(N, N)_z = -2.15$ D). The resultant is an overall CT dipole $\boldsymbol{\mu}_{CT} = +3.74–2.15 = +1.59$ D pointing in the direction expected on the basis of electronegativity difference (i.e., placing the positive end of the dipole moment vector on the side of the –N=N–), a direction which can be anticipated from the atomic charges (in a.u.: $q(F) = -0.70$, $q(N) = -0.29$, $q(C) = +1.98$).

Compared with the ground state, the excited state is characterized by a significantly higher degree of charge separation as can be gleaned from the values of the atomic charges which are (in a.u.): $q(F) = -0.76$, $q(N) = -0.39$, $q(C) = +2.30$. This means that the carbon atom has lost electronic charge ($\Delta q(C) = +0.32$ a.u.) to benefit primarily the nitrogen atoms ($\Delta q(N) = -0.10$ a.u.) followed by the fluorine atoms ($\Delta q(F) = -0.06$ a.u.)

It is the charge transfer between atomic basins rather than a change in geometry that governs the transition charge transfer dipole. This is demonstrated through a quantitative comparison of the optimized geometries of the ground and excited states. The root mean square (RMS) difference between the two sets of 15 $\{x, y, z\}$ coordinates in the two electronic states, listed in Table 5, is merely 0.0184 Å.

The charge transfer contribution of the carbon atom along the z-direction, this atom's only nonzero CT contribution, changes drastically upon excitation. This dipolar contribution flips by 180° with about the same magnitude from $\boldsymbol{\mu}_{CT}(C)_z$ (S_0) $= +0.33$ D to $\boldsymbol{\mu}_{CT}(C)_z$ (S_1) $= -0.35$ D. As already commented, the carbon atom loses 0.32 a.u. of electronic charge upon excitation, 0.12 a.u. of that is lost to the two fluorine atoms, while the remainder (0.19 a.u.) goes the two nitrogen atoms. Due to molecular geometry, the net z-projection of the charge transfers to the nitrogen atoms dominate that of the two fluorine atoms (F–C–F = 110.6°, N–C–N = 53.7°, in the ground state, with small changes in the excited state, see Fig. 2). The resulting CT term of the carbon atom in the excited state has its negative end at the side of the –N=N– moiety with respect to the xy-plane. This flipping of the direction for the CT dipole moment of the C atom upon excitation is the dominant effect that reduces the overall CT term from +1.59 D in the ground state to only +0.68 D in the excited state, a reduction by 0.91 D.

4.6 Real-space charge redistribution upon excitation

The overall characteristics of the three-dimensional redistribution of charge upon electronic excitation in difluorodiazirine are now examined. The reshaping of the electronic charge upon excitation can be visualized by examining consecutive isosurfaces of an electron density difference map. The electron density difference scalar field is defined as:

$$\Delta\rho \equiv \rho(S_1) - \rho(S_0). \tag{12}$$

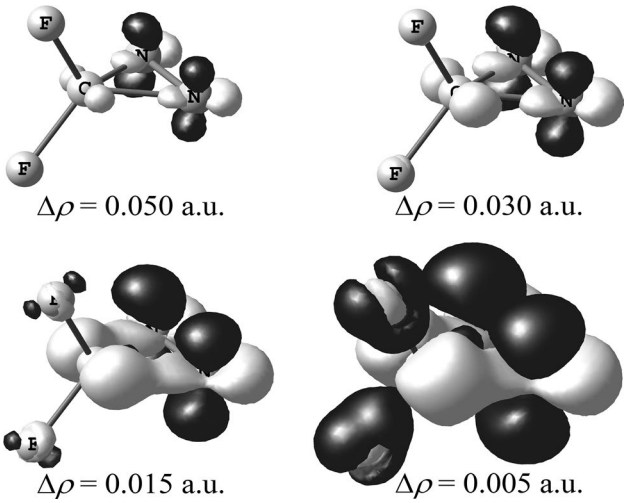

Fig. 3 Isosurfaces of the total electron density difference scalar field upon vertical excitation, $\Delta\rho = \rho(S_1) - \rho(S_0)$, superposed on a ball-and-stick model of the optimized geometry of the ground state of difluorodiazirine (CF_2N_2). The magnitudes of the plotted isosurfaces are indicated in atomic units (a.u. = e^-/bohr^3). *Darker* surfaces represent positive values (regions of electron enrichment upon excitation), and light gray regions are those representing electron depletion. Calculations were done at the (U)QCISD/aug-cc-pVTZ level of theory

Since there is no net loss or gain of electrons ($N = 38$ e^- is constant), the integral of $\Delta\rho$ over all space is zero. In other words, if electron density is lost from a region of space, it must be gained by another within the molecule.

Figure 3 depicts representations of $\Delta\rho$ for four successively decreasing values of the isosurface spanning a full order of magnitude from 0.050 to 0.005 a.u. In the figure, the dark isosurfaces denote regions of space that are enriched by electrons in the excited state while the light gray regions are the regions of electron depletion. The isosurfaces in the figure are plotted along with the molecular skeleton of the ground state, which is frozen during this vertical excitation.

The series of isosurfaces all indicate a consistent symmetry of the charge shift upon excitation. The carbon atom clearly loses electronic charge whether from regions closer to its nucleus or from more diffuse regions, consistent with a $\Delta q(C)$ of +0.32 a.u. (Table 5). The principal accumulation region of electronic charge in this transition is the –N=N– moiety, as expected for such an $n\pi^*$ transition. One can observe a loss of charge from the $\overline{C-N=N}$ plane in all depicted isosurfaces. This loss, from the sp^2 nitrogen atoms, occurs from the location of their lone pairs, with their highest density being in the plane. In addition, the figure shows that considerable charge is also lost from the

Table 6 Basic QTAIM bond critical points (BCPs), non-bonded interatomic, and ring critical points (RCPs) properties for the ground (S_0) and their changes upon vertical and adiabatic excitation ($\Delta S_{1(\text{vert})}$ and $\Delta S_{1(\text{ad})}$, respectively) of difluorodiazirine calculated at the (U) QCISD/aug-cc-pVTZ level of theory

Ω–Ω′	ρ_{CP}	$\nabla^2\rho_{CP}$	δ	ε	V_{CP}
N=N					
S_0	0.458	−1.108	1.563	0.040	−0.970
$\Delta P(S_{1(\text{vert})})$	0.006	−0.201	−0.131	−0.022	0.022
$\Delta P(S_{1(\text{ad})})$	0.005	−0.253	−0.132	−0.090	0.032
C–N					
S_0	0.311	−0.830	0.712	0.450	−0.585
$\Delta P(S_{1(\text{vert})})$	−0.008	0.235	0.054	0.557	0.028
$\Delta P(S_{1(\text{ad})})$	−0.016	0.361	0.036	0.560	0.062
C–F					
S_0	0.290	−0.016	0.574	0.277	−0.914
$\Delta P(S_{1(\text{vert})})$	0.005	−0.007	−0.019	−0.232	−0.006
$\Delta P(S_{1(\text{ad})})$	0.034	0.311	−0.028	−0.238	−0.189
F…F					
S_0			0.141		
$\Delta P(S_{1(\text{vert})})$			0.030		
$\Delta P(S_{1(\text{ad})})$			0.053		
F…N					
S_0			0.093		
$\Delta P(S_{1(\text{vert})})$			0.016		
$\Delta P(S_{1(\text{ad})})$			0.020		
C−N=N					
S_0	0.271	0.308			−0.561
$\Delta P(S_{1(\text{vert})})$	0.014	−0.152			0.033
$\Delta P(S_{1(\text{ad})})$	0.006	−0.139			0.058

The electron density and its Laplacian and the potential energy density at the (bond or ring) critical point, ρ_{CP}, $\nabla^2\rho_{CP}$, and V_{CP}, respectively, are in atomic units (a.u.), while the ellipticity ε and the delocalization index ($\delta(\Omega,\Omega')$) are dimensionless. The change in a property is defined as the difference between a given parameter (P) in the excited state $P(S_1)$ minus its value in the ground state $P(S_0)$, that is, $\Delta P = P(S_1) - P(S_0)$

region that connects the carbon atom to each nitrogen and contains the C–N bond paths, weakening the bonds.

Table 6 lists some of the basic QTAIM bond, interatomic (delocalization), and ring descriptors for the ground state and their changes upon excitation, both vertical and adiabatic. The investigated properties include the electron density ρ at critical points (CPs) (bond critical points (BCPs) and ring critical point (RCP)), the Laplacian of the total electron density at the bond and ring critical points ($\nabla^2\rho_{BCP}$ and $\nabla^2\rho_{RCP}$, respectively), the electron delocalization index, $\delta(\Omega,\Omega')$, which counts the number of electrons shared between any two atoms in the molecule whether they share a bond path or not, the ellipticity (defined in terms of the ratio of the two principal negative curvatures at the bond critical point, $\varepsilon = \lambda_1/\lambda_2 - 1 \geq 0$, which measures the departure of the electron density at the BCP from cylindrical symmetry with a value of 0 indicating perfect cylindrical symmetry), and the potential energy density at the CP, V_{CP}.

An examination of Table 6 reveals that the loss of electron density from the C–N bonding region, apparent in all plotted isosurfaces of Fig. 3, is reflected in a lower electron density, a higher potential energy density, and a higher ellipticity at the corresponding BCPs. Thus, upon vertical excitation, $\Delta\rho_{BCP}(S_{1(\text{vert})}) \approx -0.01$ a.u., a value that reaches −0.02 a.u. when the geometry is relaxed, which suggests weaker C–N bonds in the excited state. The lower electron density at the BCP in the C–N bond is accompanied by a rise in the potential energy density at that point, $\Delta V_{BCP}(S_{1(\text{vert})}) \approx 0.03$ a.u. and $\Delta V_{BCP}(S_{1(\text{ad})}) \approx 0.06$ a.u., which indicates a local relative destabilization of this bond path. For this bond, the Laplacian is still negative in the excited state (both vertical and adiabatic) but with a smaller magnitude indicating a flatter density at the BCP region. These observations together with the increased ellipticity point at a weakening of the C–N bond upon excitation which is consistent with the observed reactivity of difluorodiazirine expressed in reaction (1).

Figure 3 suggests that the principal gain in electronic charge from the redistribution of the electron density occurs in the region of the –N=N– fragment whereby the electron enrichment occurs symmetrically above and below the ring plane, i.e., has π-symmetry, as may be expected for an $n\pi^*$ transition. This primary gain of electron density by the N_2 moiety is consistent with the changes in integrated QTAIM charges that indicate that nitrogen is the atom most enriched in electron population due to the (adiabatic) excitation—Table 5. Given that the enrichment of the –N=N– fragment is not occurring within the ring plane, the ρ_{BCP}(N=N) hardly changes upon excitation, increasing by only 0.006 (vertical)/0.005 (adiabatic) a.u., while the Laplacian is significantly more negative.

The fluorine atoms also gain electronic population but only in the more diffuse regions as can be seen from the difference electron density maps presented in Fig. 3. Meanwhile, the C–F bonds gain considerable stability once the geometry is allowed to relax as can be inferred from a shorter bond length, a higher electron density accompanied with a lower potential energy density at the BCP, a lower ellipticity, and a higher degree of electron sharing (albeit marginal) in the excited state. Thus, all indicators point to a stronger C–F bond in the excited state, which can also be gleaned visually from the most diffuse envelope in Fig. 3 (the 0.005 envelope) that places density in the C–F bonding region. Interestingly, the Laplacian of the density at the BCP of the C–F bond become slightly more negative upon vertical excitation but reverses sign and reach a positive value of 0.296 a.u. upon geometry relaxation of the excited state.

The inversion of the sign of the Laplacian may reflect the much higher ionicity of this bond in the adiabatic excited state as the difference in the charges of the bonded atoms, $q(\mathrm{F}) - q(\mathrm{C})$, reaches −3.060 a.u. in the adiabatically excited state when it only equals −2.680 a.u. in the ground state.

The picture that emerges from the analysis of QTAIM bond properties points to a weakening of the C–N bonds with an accompanying strengthening of C–F bonds on excitation favoring the products of Reaction (1).

To obtain further insight into the charge redistribution upon excitation, the topography of the Laplacian of the total electron density ($\nabla^2\rho$) scalar field is now examined. It is well known that regions where $\nabla^2\rho > (<)\ 0$ are regions of local depletion (concentration) of the electron density relative to its average distribution that act as acidic (basic) region in the Lewis sense. A chemical reaction proceeds by aligning an attacking "lump" in the valence shell charge concentration (VSCC) of a Lewis base region in a donor with a "hole" in the VSCC of an acidic region in an acceptor [18].

Atoms that are covalently bonded exhibit a charge concentration in the bonding region and hence a negative Laplacian at the BCP. Charge concentrations can also be observed in regions that are normally associated with lone pairs. This latter observation is a manifestation of what is termed "partial pair condensation," that is, regions of space where the probability of occupation by a single pair of electrons is greater than the molecular average [64, 65]. The Laplacian of the electron density provides an approximate mapping of electron pairing determined in the six-dimensional space of the pair density onto the real three-dimensional space of the electron density [65].

Figure 4 displays the Laplacian scalar field ($\nabla^2\rho$) in the ring plane of both the ground and excited states of difluorodiazirine. The region expected for the partial pair condensation associated with the lone pairs on the nitrogen atoms in the ground state is displayed in the figure as an isosurface ($\nabla^2\rho = -2.0$ a.u.) that encloses a negative region of local charge concentration associated with each one of the two nitrogen atoms (Fig. 4a). This isosurface disappears completely upon excitation as shown in Fig. 4b where now the most negative contour surrounding the negative region is of magnitude of only 0.8 a.u., indicating the loss of the former partial pair condensation from the ring plane due to the $n\pi^*$ excitation.

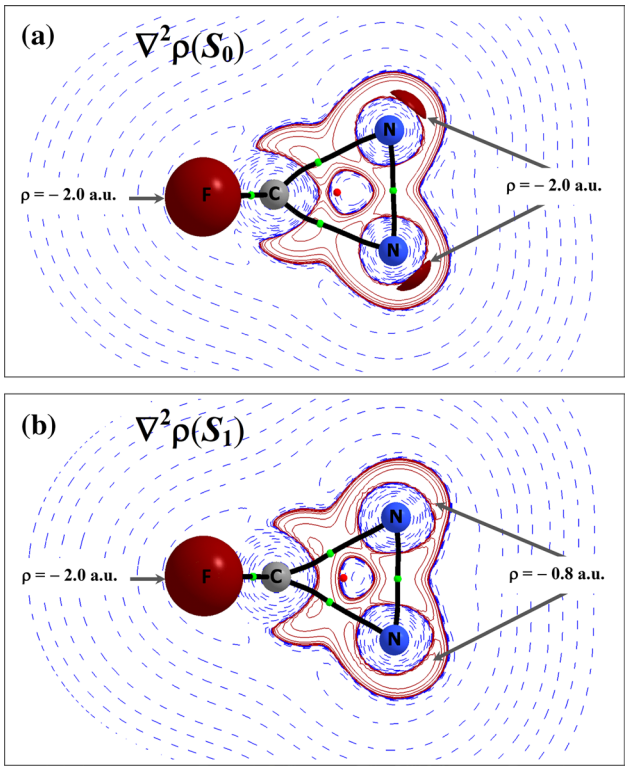

Fig. 4 Laplacian of the electron density ($\nabla^2\rho$) in the N–C–N plane of difluorodiazirine in its ground and vertically excited state (S_0 and S_1, respectively). **a** Contours of $\nabla^2\rho$ in S_0 along with the $\nabla^2\rho = -2.0$ a.u. isosurface at the anticipated position of the lone pair of each nitrogen atom. The $\nabla^2\rho = -2.0$ a.u. isosurface also surrounds the two fluorine atoms (only one F atom is shown as the second is eclipsed in this view). Each F atom has a second internal isosurface of $\nabla^2\rho = -2.0$ a.u. hidden by the external solid isosurface. **b** Contours of $\nabla^2\rho$ in the vertically excited S_1 state with the same selected isosurface ($\nabla^2\rho = -2.0$ a.u.) enclosing the fluorine atoms, but no longer exhibits the charge concentrations attributed to the lone pairs. The contour enclosing the lone pair regions is now of a magnitude of only 0.8 a.u. (instead of 2.0 a.u. in S_0). (*Dashed blue* contours depict $\nabla^2\rho > 0$, while red solid contours depict $\nabla^2\rho < 0$. Contours start from the outside inward with magnitudes: 0.001, 0.002, 0.004, 0.008, 0.02, 0.04, 0.08, 0.2, 0.4, 0.8, 2, 4, 8, 20 a.u. Calculations were done at the (U) QCISD/aug-cc-pVTZ level of theory)

4.7 Changes in the molecular electrostatic potential (ESP) upon excitation

Recently, Kim et al. [56] studied the molecular electrostatic potential (ESP) and the dipole moment of carbon monoxide in its ground ($X\ ^1\Sigma^+$) and excited triplet ($^3\Pi$) states at the CCSD(T)/aV5Z level of theory. At this level of theory, the reported dipole moment magnitude is 0.11 D and points its positive end toward the oxygen atom ($^-\overrightarrow{C=O}^+$) [56] consistent with well-known experimental and computational results. Kim et al. then find that, in the ground state, the ESP of CO exhibits negative regions at both atom ends with the carbon end having more negative values. In other words, a positively charged species approaching along the molecular axis would favor the carbon atom over the oxygen atom. In contrast, a negative reactant would approach the cylindrical surface surrounding the bond as it exhibits a positive ESP. The topography of the ESP is, hence, dominated by two nodal surfaces separating the end-atom regions from the region concentric with the C–O bond axis.

In the excited triplet state of CO, the calculated dipole moment is reversed with its negative pole on the side of the

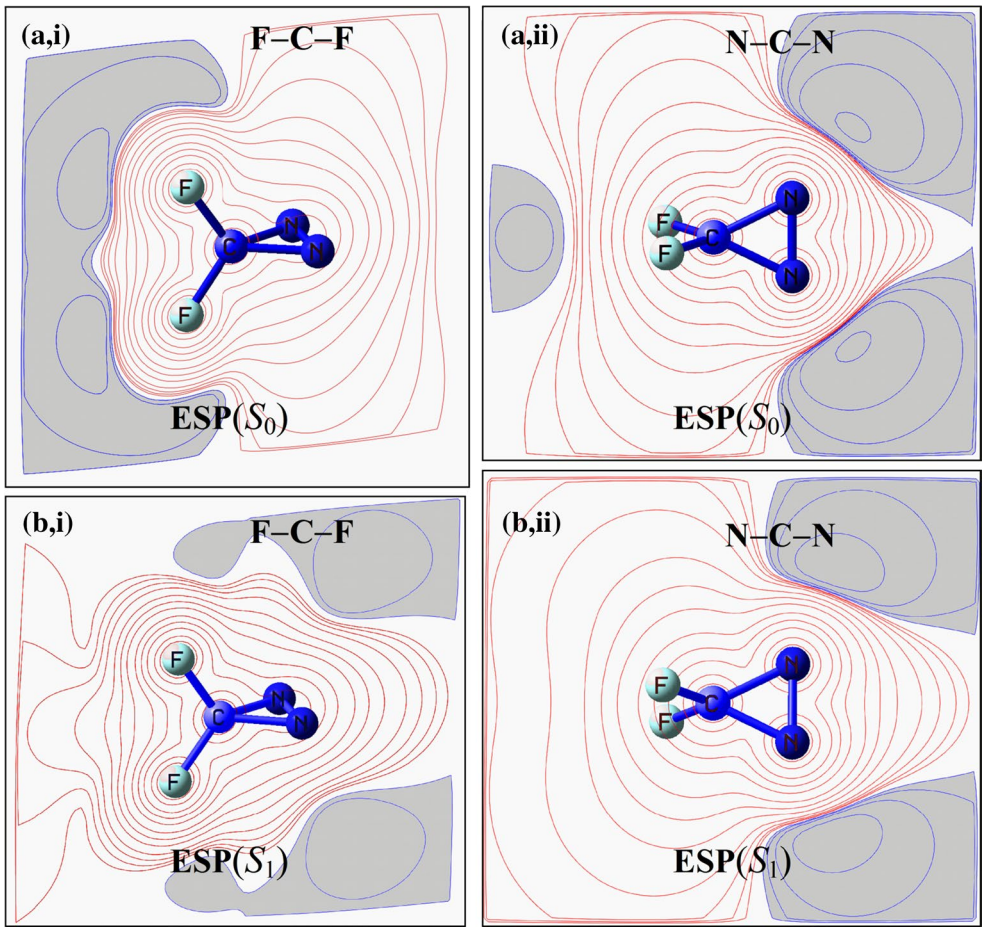

Fig. 5 Contour maps of the molecular electrostatic potential (ESP) of difluorodiazirine in its ground and vertically first singlet excited state (S_0 and S_1, respectively). The *top panel* (**a**) represents the contours of the ESP in S_0, while the *bottom panel* (**b**) shows the respective contours for the vertically excited state S_1. Every panel consists of a plot in the σ_v' plane (the F–C–F plane) (***i***) and in the σ_v (the N–C–N ring plane) (***ii***), and both planes are slightly tilted in the figure for a better view. Contours of regions shaded in dark gray (with *blue contour lines*) depict regions of negative ESP, while the light regions (with *red contour lines*) are those where the ESP is positive. (Contours start from the outside inwards with magnitudes of 0.001, 0.002, 0.004, 0.008, 0.02, 0.04, 0.08, 0.2, 0.4, 0.8, 2, 4, 8, 20 a.u. Calculations were done at the (U)QCISD/aug-cc-pVTZ level of theory)

oxygen atom $^{+}\overleftarrow{C=O}^{-}$ and with a (substantial) magnitude of 1.39 D (CCSD(T)/aV5Z) [56]. The triplet CO is found to exhibit a positive ESP at the carbon end and a negative ESP at the oxygen end. This considerable reorganization of the topography of the ESP is accompanied with the replacement of the two nodal surfaces observed in the ground state by only one nodal surface separating the positive region surrounding the carbon atom from the negative one surrounding the oxygen atom.

There are some parallels between difluorodiazirine and CO, and these are: (1) Both ground states have very small or vanishing dipole moments despite of the fact that the two molecules are composed of atoms with highly different electronegativities and (2) a significant dipole moment arises upon electronic excitation of these two molecules.

Given the above similarities in the dipolar behavior of the two molecules, and following the lead of Kim et al., the changes in the ESP of diazirine accompanying electronic excitation are now explored. Representations of difluorodiazirine's ESP in the ground and excited states in the two symmetry planes σ_v (the $\overline{C-N=N}$ ring plane) and in the σ_v' plane (the F–C–F plane) are shown in Fig. 5.

The left of the top panel in Fig. 5 represents the ESP in the σ_v' plane and shows a region of negative ESP at the side of the fluorine atoms leaving the rest of the plane to exhibit positive ESP contours throughout. Upon rotation by 90° around the z-axis to the ring σ_v plane, one notes a remnant of the negative region from the side of the fluorine atoms along the bisector of the F–C–F angle. More importantly, the ring plane features two dominant negative

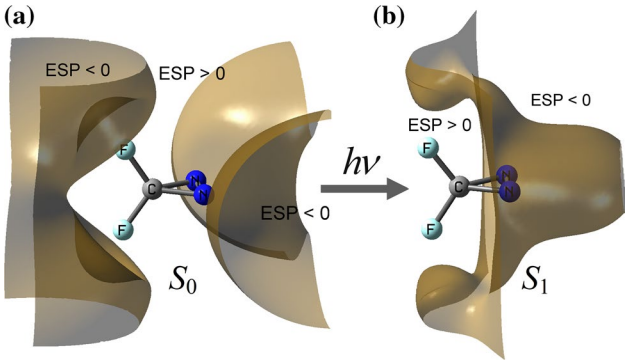

Fig. 6 Nodal surfaces in the molecular electrostatic potential (ESP) of difluorodiazirine in its ground and vertically excited state, S_0 (**a**) and S_1 (**b**), respectively. (Calculations were done at the (U)QCISD/aug-cc-pVTZ level of theory)

regions characteristic of the lone pairs of the two sp^2 nitrogen atoms, and the two regions merge at large distances from the molecule. The topography of the ESP scalar field is, thus, characterized by two infinite nodal surfaces separating two regions of negative ESP at the molecule's end (along the extremities of the C_2 axis (z-axis)) from a midsection of positive electrostatic potential. The two nodal surfaces in the ESP of the ground-state difluorodiazirine are displayed in Fig. 6a. Beside the distortion of the form of the nodal surfaces dictated by the geometry and symmetry of difluorodiazirine, this topography is reminiscent of that of the ground state of CO reported by Kim et al. [56].

The ESP of the vertically first excited singlet state of difluorodiazirine has a different topography governed completely by the redistribution of electronic charge in the excited state (no nuclear contribution to the change in the ESP here since the molecular skeleton is frozen). A striking change in the excited state ESP is the disappearance of the negative region from the side of the fluorine atoms in both perpendicular planes and the appearance of negative ESP above and below the N=N bond as shown in Fig. 5b,i. Concomitant with this appearance of negative ESP above and below the nitrogen atoms is the significant reduction in the magnitude of the negative ESP that was ascribed to the lone pair in the ground state (due to the $n\pi^*$ excitation). The net result of these changes is the replacement of the two nodal surfaces of the ground state with only one in the excited state that separates a negative potential region at the side of the nitrogen atoms from a positive region elsewhere (Fig. 6b).

5 Conclusions

A real-space explanation for the null dipole moment of difluorodiazirine in the ground state and its sharp change upon its spin-allowed electronic excitation is presented. This orbital-free explanation is formulated in terms of a quantum mechanical observable [58, 59], that is, the electron density, a quantity accessible from both theory [18] and from experiment [60–62]. The weakening of the C–N bonds upon excitation, as indicated by the QTAIM bond properties, is consistent with favoring reaction (1) to proceed in the forward direction to produce the difluorocarbene radical ($:CF_2$) upon flash photolytic decomposition of 3,3′-difluorodiazirine (CF_2N_2).

The observed lack of a dipole moment for the ground state of this molecule is the result of a cancelation between the charge transfer and atomic polarization dipolar contributions. This balance of opposite contributions is disturbed upon excitation due to the flow of electronic charge toward the –N=N– moiety. This charge flow leads to a dramatic change in the charge transfer term without affecting the atomic polarization significantly. Since the two contributions are opposite in sign, this reduces the cancelation that exists in the ground state leading to the observed dipole moment in the excited state (which points its negative end toward the nitrogen atoms).

This decomposition/reconstruction of the dipole moment in the first singlet excited state of difluorodiazirine does not require more than the charge density. No explicit reference is made anywhere to the full density matrix nor to any particular molecular orbital or set of orbitals. The electronic structure calculation was merely used to generate the density, but this density could have been obtained from X-ray diffraction with the possible prohibition of only technical difficulties such as crystallization and/or lifetime problems. This is the strength of this approach, namely that it results from a real-space orbital-free analysis of a quantum observable, the electron density, and equivalently the total *charge* density (including the point-like nuclear charge distribution) and its associated electrostatic potential.

Finally, a comparison of calculated spectroscopic, geometric, and electric properties of difluorodiazirine with experiment in both the ground and the first singlet excited states demonstrates that the level of theory denoted as (U)QCISD/aug-cc-pVTZ is adequate to study this molecule. This result can be useful if this real-space approach is adopted in the study of substituted diazirines.

Note added in proof A study of the different reaction channels and their corresponding potential energy surfaces of dissociation of several diazirines have just appeared. The reported calculations at the composite level of theory G3 are in good agreement with experimental kinetic results which supports the mechanisms proposed by the authors [67].

Acknowledgments The authors thank the two anonymous reviewers especially Reviewer #1 who suggested the examination of the Laplacian scalar field and its change upon excitation. The authors also thank Professor Lou Massa (Hunter College, City University of New York), Professor Paul W. Ayers (McMaster University), and Drs. Jim Hess and Douglas J. Fox of Gaussian, Inc., for helpful comments. L.A.T. thanks CAPES for a doctoral fellowship and CNPq (*Science without Borders Scholarship Program*—205445/2014-4) and for a Visiting Graduate Studentship at *Mount Saint Vincent University*. R. L. A. H thanks FAPESP for financial support (Grants 2014/23714-1 and 2010/18743-1, São Paulo Research Foundation). C. F. M. acknowledges the funding of the *Natural Sciences and Engineering Research Council of Canada* (NSERC), *Canada Foundation for Innovation* (CFI), and *Mount Saint Vincent University* for financial support.

References

1. Mitsch RA (1965) J Am Chem Soc 87:758–761
2. Mitsch RA (1964) J Heterocycl Chem 1:271–274
3. Dubinsky L, Krom BP, Meijler MM (2012) Bioorg Med Chem 20:554–570
4. Bjork CW, Craig NC, Mitsch RA, Overend J (1965) J. Am. Chem. Soc. 87; 1186–1191 (captions of Figs. 1 and 2 in this reference should be switched as described in a correction by the authors in a citation of this article as Ref. [1], p. 897, in: Norman CR, Kliewer MA (1979) Spectrochim. Acta 35A; 895–897)
5. Douglas MM (1966) United States Patent US3257381A
6. Moss RA, Wang L, Krogh-Jespersen K (2009) J Am Chem Soc 131:2128–2130
7. Bogey M, Winnewisser M, Christiansen JJ (1984) Can J Phys 62:1198–1216
8. Hencher JL, Bauer SH (1967) J Am Chem Soc 89:5527–5531
9. Craig NC, Kliewer MA (1979) Spectrochim Acta A 35A:895–897
10. Sieber H, Neusser HJ, Stroh F, Winnewisser M (1991) J Mol Spectr 148:453–461
11. Pandey RR, Khait YG, Hoffmann MR (2004) J Phys Chem A 108:3119–3124
12. Sieber H, Riedle E, Neusser HJ (1990) Chem Phys Lett 169:191–197
13. Lombardi JR, Klemperer W, Robin MB, Basch H, Kuebler NA (1969) J Chem Phys 51:33–44
14. Hollas JM, Hepburn PH (1974) J Mol Spect 50:126–141
15. Hollas JM (1982) High resolution spectroscopy. Butterworths, London
16. Pauling L (1960) The nature of the chemical bond, 3rd edn. Cornell University Press, Ithaca
17. Pople JA, Head-Gordon M, Raghavachari K (1987) J Chem Phys 87:5968–5975
18. Bader RFW (1990) Atoms in molecules: a quantum theory. Oxford University Press, Oxford
19. Popelier PLA (2000) Atoms in molecules: an introduction. Prentice Hall, London
20. Matta CF, Boyd RJ (eds) (2007) The quantum theory of atoms in molecules: from solid state to dna and drug design. Wiley-VCH, Weinheim
21. Hovick JW, Poler JC (2005) J Chem Educ 82:889
22. Coulson CA (1961) Electricity. Oliver and Boyd, London
23. Turro NJ (1991) Modern molecular photochemistry. University Science Books, Sausalito
24. Simmons JD, Bartky IR, Bass AM (1965) J Mol Spectrosc 17:48–49
25. Bakhsliev NG, Knyazhanskii MI, Minkin VI, Osipov OA, Saidov GV (1969) Russ Chem Rev 38:740–754
26. Bader RFW, Bayles D, Heard GL (2000) J Chem Phys 112:10095–10105
27. Buttingsrud B, Alsberg BK, Åstrand P-O (2007) Phys Chem Chem Phys 9:2226–2233
28. Gutiérrez-Arzaluz L, Cortés-Guzmán F, Rocha-Rinza T, Peón J (2015) Phys Chem Chem Phys (PCCP) 17:31608–31612
29. Jenkins S, Blancafort L, Kirk SR, Bearpark MJ (2014) Phys Chem Chem Phys (PCCP) 16:7115–7126
30. Sánchez-Flores EI, Chávez-Calvillo R, Keith TA, Cuevas G, Rocha-Rinza T, Cortés-Guzmán F (2014) J Comput Chem 35:820–828
31. Jara-Cortés J, Rocha-Rinza T, Hernández-Trujillo J (2015) Comput Theor Chem 1053:220–228
32. Syrkin YK, Dyatkina ME (1964) Structure of molecules and the chemical bond (english translation). Dover Publications Inc, New York
33. Davies M (1965) Some electrical and optical aspects of molecular behaviour. Pergamon Press, Oxford
34. Laidig KE, Bader RFW (1990) J Chem Phys 93:7213–7224
35. Bader RFW, Keith TA (1993) J Chem Phys 99:3683–3693
36. Bader RFW (2002) Mol Phys 100:3333–3344
37. Bader RFW, Matta CF (2001) Int J Quantum Chem 85:592–607
38. Matta CF, Sowlati-Hashjin S, Bandrauk AD (2013) J Phys Chem A 117:7468–7483
39. Keith TA (2007) Chapter 3. In: Matta CF, Boyd RJ (eds) The quantum theory of atoms in molecules: from solid state to DNA and drug design. Wiley-VCH, Weinheim
40. Dunning TH (1989) J Chem Phys 90:1007–1023
41. Szabo A, Ostlund NS (1989) Modern quantum chemistry: introduction to advanced electronic structure theory. Dover Publications Inc, New York
42. Møller C, Plesset MS (1934) Phys Rev 46:618–622
43. Scuseria GE, Janssen CL, Schaefer HF III (1988) J Chem Phys 89:7382–7387
44. Purvis GD III, Bartlett RJ (1982) J Chem Phys 76:1910–1918
45. Shavitt I, Bartlett RJ (2009) Many-body methods in chemistry and physics: mbpt and coupled-cluster theory. Cambridge University Press, Cambridge
46. Parr RG, Yang W (1989) Density-functional theory of atoms and molecules. Oxford University Press, Oxford
47. Koch W, Holthausen MC (2001) A chemist's guide to density functional theory, 2nd edn. Wiley-VCH, New York
48. Becke A (1993) J Chem Phys 98:5648–5652
49. Lee C, Yang W, Parr R (1988) Phys Rev B 37:785–789
50. Jablonski M, Palusiak M (2010) J Phys Chem A 114:12498–12505
51. Rykounov AA, Tsirelson VG (2009) J Mol Struct (Theochem) 906:11–24
52. Matta CF (2010) J Comput Chem 31:1297–1311
53. Frisch MJ, Trucks GW, Schlegel HB, Scuseria GE, Robb MA, Cheeseman JR, Scalmani G, Barone V, Mennucci B, Petersson GA, Nakatsuji H, Caricato M, Li X, Hratchian HP, Izmaylov AF, Bloino J, Zheng G, Sonnenberg JL, Hada M, Ehara M, Toyota K, Fukuda R, Hasegawa J, Ishida M, Nakajima T, Honda Y, Kitao O, Nakai H, Vreven T, Montgomery Jr JA, Peralta JE, Ogliaro F, Bearpark M, Heyd JJ, Brothers E, Kudin KN, Staroverov VN, Keith T, Kobayashi R, Normand J, Raghavachari K, Rendell A, Burant JC, Iyengar SS, Tomasi J, Cossi M, Rega N, Millam JM, Klene M, Knox JE, Cross JB, Bakken V, Adamo C, Jaramillo J, Gomperts R, Stratmann RE, Yazyev O, Austin AJ, Cammi R, Pomelli C, Ochterski JW, Martin RL, Morokuma K, Zakrzewski VG, Voth GA, Salvador P, Dannenberg JJ, Dapprich S, Daniels AD, Farkas O, Foresman JB, Ortiz JV, Cioslowski J, Fox DJ

(2010) Gaussian 09, Revision B.01. Gaussian Inc.: Wallingford CT
54. Keith TA (2015) AIMAll/AIMStudio (http://aim.tkgristmill.com/)
55. Frenking G, Loschen C, Krapp A, Fau S, Strauss SH (2007) J Comp Chem 28:117–126
56. Kim H, Doan VD, Cho WJ, Valero R, Tehrani ZA, Madridejos JML, Kim KS (2015) Sci Rep 5:16307
57. Matta CF, Gillespie RJ (2002) J Chem Educ 79:1141–1152
58. Bader RFW, Zou PF (1992) Chem Phys Lett 191:54–58
59. Bader RFW, Matta CF (2004) J Phys Chem A 108:8385–8394
60. Tsirelson VG, Ozerov RP (1996) Electron density and bonding in crystals: principles, theory and x-ray diffraction experiments in solid state physics and chemistry. Institute of Physics Publishing, New York
61. Koritsanszky TS, Coppens P (2001) Chem Rev 101:1583–1628
62. Coppens P (1997) X-ray charge densities and chemical bonding. Oxford University Press Inc, New York
63. Sturm JE (1990) J Chem Educ 67:32–33
64. Bader RFW (2000) Coord Chem Rev 197:71–94
65. Bader RWF, Heard GL (1999) J Chem Phys 111:8789–8797
66. National Institute of Standards and Technology (NIST) (2015) Computational Chemistry Comparison and Benchmark DataBase: Precomputed vibrational scaling factors (http://cccbdb.nist.gov/vibscale.asp)
67. Avendaño M, Cordova T, Mora JR, Chuchani G (2016) Comput Theor Chem 1078:23–29